IMPROVEMENTS IN LINEAR BUCKLING AND GEOMETRIC NONLINEAR ANALYSIS FOR MSC/NASTRAN'S SHELL ELEMENTS

Claus C. Hoff

The MacNeal-Schwendler Corporation,
815 Colorado Blvd.,
Los Angeles, CA 90041.

ABSTRACT

This paper presents an improved approach for linear buckling and geometric nonlinear analysis in MSC/NASTRAN. The differential stiffness and the internal forces of the QUAD4 and TRIA3 shell elements have been corrected in MSC/NASTRAN Version 68. The linear stiffness of the shell elements has not been changed. With the corrections in Version 68, two major capabilities have been improved. The eigenproblem in linear buckling analysis of thin shells is free of spurious modes which have been observed in Version 67.5 and earlier Versions. Furthermore, the shell elements converge better in geometric nonlinear analysis. The theoretical concept of the corotational formulation in MSC/NASTRAN is summarized briefly. The corrections of the internal forces and tangent stiffness are explained. Examples are presented which illustrate the improved behavior of the shell elements in Version 68 as compared to Version 67.5.

Introduction

For some problems, the geometric nonlinear capability has not performed satisfactory in MSC/NASTRAN Version 67.5 and earlier. In 1991, Dr.MacNeal reviewed the theory for geometric nonlinear analysis, see [1]. It was found that the internal forces were inconsistent with the principle of virtual work in case of large displacements and large rotations. Improved formulas based on revised internal forces were derived for elastic and differential stiffness. The theoretical results in [1] have been confirmed by numerical experiments. Accordingly, it has been decided to improve the geometric nonlinear capability of the QUAD4 and TRIA3 shell elements in Version 68 of MSC/NASTRAN.

MSC/NASTRAN uses the so called corotational formulation in geometric nonlinear analysis. The average rigid body motion of a finite element is condensed out of the total deformations and only the remaining net deformations (distortions) are considered in the strain energy of the element. If we assume that the element distortions remain small, a linear strain measure in the element is sufficient even for large overall deformations.

The main difficulty in the corotational formulation is the linearization of the virtual work terms in closed form. Nour-Omid and Rankin developed a generic method to linearize elements with a corotational formulation, see [2] and [3]. We found that the formulas of the internal force and tangent stiffness derived by Dr.MacNeal in [1] correspond to the formulas in [2] and [3]. In [1], [2], and [3], the term with the internal virtual work is linearized in its discrete form using virtual deformations and internal forces of the element grid points, respectively. Crisfield shows, in his textbook [4], that the linearization of the discrete form is equivalent to the linearization of the continuum form of the virtual work equation.

The approach taken in this paper does not change the linear behavior of the shell elements. The corrections of the internal forces, the correction of the linear stiffness and the new calculation of the differential stiffness are implemented as postprocessors to the existing element processors, see [5] for details.

In the following chapters, we summarize the corotational concept which has been used in all MSC/NASTRAN nonlinear elements except in the new hyperelastic elements of Version 67.5 and 68. The correction of the internal forces and the linear stiffness and the calculation of the differential stiffness are explained. Examples are presented which illustrate the improvements in linear buckling and geometric nonlinear analysis.

The Corotational Concept in MSC/NASTRAN

In the corotational concept of MSC/NASTRAN, the average rigid body motion of an element is condensed out of the total deformation. The displacement of the element origin, usually an element grid point, is considered to be the average rigid body translation of the element, see Figure 1. The rotation of the element base vectors from the undeformed to the deformed position is considered to be the average rigid body rotation of the element. The rigid body rotation of the element in components of the basic system (b) is

$$\mathbf{R}_D^{(b)} = \mathbf{T}_{bd}^{(b)} \mathbf{T}_{be}^{(b)T} \tag{1}$$

with

$$\mathbf{T}_{bd}^{(b)} = \left[\mathbf{d}_1^{(b)} \middle| \mathbf{d}_2^{(b)} \middle| \mathbf{d}_3^{(b)} \right] \qquad \mathbf{T}_{be}^{(b)} = \left[\mathbf{e}_1^{(b)} \middle| \mathbf{e}_2^{(b)} \middle| \mathbf{e}_3^{(b)} \right] \tag{2}$$

where $\mathbf{T}_{be}$, and $\mathbf{T}_{bd}$ are transformation matrices from the basic system to the undeformed and deformed element system, respectively. The vectors $\mathbf{e}_i$, and $\mathbf{d}_i$ are the orthogonal unit base vectors of the undeformed and deformed element triads, respectively. The rigid body rotation angles $\boldsymbol{\omega}_D$ are calculated from the rotation matrix

$$\mathbf{R}_D = e^{spin\,\boldsymbol{\omega}_D} \tag{3}$$

$$spin(\boldsymbol{\omega}_D) := \begin{bmatrix} 0 & -\omega_{D3} & \omega_{D2} \\ \omega_{D3} & 0 & -\omega_{D1} \\ -\omega_{D2} & \omega_{D1} & 0 \end{bmatrix} \tag{4}$$

The element net displacements of grid point I in (b) components are

$$\overline{\mathbf{u}}_I^{(b)} = \mathbf{x}_e^{I(b)} - \mathbf{R}_D^{(b)} \mathbf{X}_e^{I(b)} \tag{5}$$

or in (d) components

$$\overline{\mathbf{u}}_I^{(d)} = \mathbf{x}_e^{I(d)} - \mathbf{X}_e^{I(e)} \tag{6}$$

with

$$\mathbf{x}_e^{I(b)} = \mathbf{x}^{I(b)} - \mathbf{x}^{0(b)} \tag{7}$$

$$\mathbf{X}_e^{I(b)} = \mathbf{X}^{I(b)} - \mathbf{X}^{0(b)} \tag{8}$$

$\mathbf{X}^{I(b)}$ is the undeformed position of grid point I with respect to the origin of the basic system, $\mathbf{X}_e^{I(b)}$ is the undeformed position of grid point I with respect to the origin of the undeformed element system. Bolded upper case letters refer to the undeformed configuration, bolded lower case letter refer to the deformed configuration. Superscript 0 denotes the element origin, superscript (b), (e), and (d) denote components in the basic, undeformed element, and deformed element system, respectively. Note that eqn(6) is written in mixed components.

The rotation matrix of the element net rotations of grid I in (d) components is

$$\overline{\mathbf{R}}_I^{(d)} = \mathbf{T}_{bd}^{(b)\,T}\, \mathbf{R}_I^{(b)}\, \mathbf{T}_{be}^{(b)} \tag{9}$$

where $\mathbf{R}_I^{(b)}$ is the rotation matrix of the overall rotations $\boldsymbol{\omega}_I^{(b)}$ in the basic system, and $\overline{\mathbf{R}}_I^{(d)}$ is the roation matrix of the element net rotation $\overline{\boldsymbol{\omega}}_I^{(d)}$ in the deformed element system.

The net displacements $\overline{\mathbf{u}}_I^{(d)}$ and the net rotations $\overline{\boldsymbol{\omega}}_I^{(d)}$ are now free of rigid body translations $(\mathbf{x}^0 - \mathbf{X}^0)$ and free of rigid body rotations $\boldsymbol{\omega}_D$.

Correction of the Internal Forces

The virtual work of the internal forces $\mathbf{f}_I$ has to be invariant for rigid body motion. If we have internal forces $\overline{\mathbf{f}}_I$ which do not satisfy invariance, we enforce the following equivalence in the virtual work

$$\delta\overline{\mathbf{d}}_I^T\, \overline{\mathbf{f}}_I = \delta\mathbf{d}_I^T\, \mathbf{f}_I\,; \qquad I = 1,...N \tag{10}$$

with

$$\mathbf{d}_I := \left\{ \begin{array}{c} \mathbf{u}_I \\ \boldsymbol{\omega}_I \end{array} \right\} \{6\}\,; \qquad \overline{\mathbf{d}}_I := \left\{ \begin{array}{c} \overline{\mathbf{u}}_I \\ \overline{\boldsymbol{\omega}}_I \end{array} \right\} \{6\} \tag{11}$$

and

$$\mathbf{f}_I := \left\{ \begin{array}{c} \mathbf{n}_I \\ \mathbf{m}_I \end{array} \right\} \{6\} \tag{12}$$

Starting with eqn (10), all quantities in this paper are in the deformed element sytem (d) if not indicated otherwise. N denotes the number of grid points in the element,

$\mathbf{u}_I = \mathbf{x}_e^I - \mathbf{X}_e^I$ are the element displacements without rigid body translation, $\boldsymbol{\omega}_I$ are the overall rotations, $\mathbf{n}_I$ are the normal and shear forces, $\mathbf{m}_I$ are the moments. Repeated indices in upper case letters indicate sum over the grid points from 1 to N. In (10), we assume that the forces $\bar{\mathbf{f}}_I$ are already invariant for rigid body translation. From(10), we get the corrected forces

$$\mathbf{f}_I = \mathbf{P}_{KI}^T \, \bar{\mathbf{f}}_K \tag{13}$$

with

$$\mathbf{P}_{IJ} = \frac{\partial \bar{\mathbf{d}}_I}{\partial \mathbf{d}_J} = \left[\begin{array}{c|c} \dfrac{\partial \bar{\mathbf{u}}_I}{\partial \mathbf{u}_J} & \dfrac{\partial \bar{\mathbf{u}}_I}{\partial \boldsymbol{\omega}_J} \\ \hline \dfrac{\partial \bar{\boldsymbol{\omega}}_I}{\partial \mathbf{u}_J} & \dfrac{\partial \bar{\boldsymbol{\omega}}_I}{\partial \boldsymbol{\omega}_J} \end{array}\right] \quad [6,6] \tag{14}$$

The matrix $\mathbf{P}_{IJ}$ is called a projection matrix according to [2] and [3] because it projects out the rigid body mode components. The corrected internal forces $\mathbf{f}_I$ satisfy equilibrium in the deformed element.

The corrected element forces are transformed from the deformed element system (d) to the basic system (b) and then assembled in a sum over the elements.

$$\mathbf{f}_I^{(b)} = \mathbf{D}_{bd}^{(b)} \, \mathbf{P}_{KI}^{(d)T} \, \bar{\mathbf{f}}_K^{(d)} \tag{15}$$

with

$$\mathbf{D}_{bd}^{(b)} = \begin{bmatrix} \mathbf{T}_{bd}^{(b)} & \mathbf{0} \\ \mathbf{0} & \mathbf{T}_{bd}^{(b)} \end{bmatrix} \tag{16}$$

Correction of the Tangent Stiffness

The variation of the internal forces $\mathbf{f}_I^{(b)}$ with respect to the deformations $\mathbf{d}_J^{(b)}$ is

$$\delta \mathbf{f}_I^{(b)} = \mathbf{D}_{bd} \, \mathbf{P}_{KI}^{(d)T} \, \delta \bar{\mathbf{f}}_K^{(d)} + \mathbf{D}_{bd} \, \delta \mathbf{P}_{KI}^{(d)T} \, \bar{\mathbf{f}}_K^{(d)} + \delta \mathbf{D}_{bd} \, \mathbf{P}_{KI}^{(d)T} \, \bar{\mathbf{f}}_K^{(d)} \tag{17}$$

The tangent stiffness is defined to be

$$\mathbf{K}_{IJ}^{(b)} := \frac{\partial \mathbf{f}_I^{(b)}}{\partial \mathbf{d}_J^{(b)}} \qquad [6,6] \tag{18}$$

In MSC/NASTRAN, the tangent stiffness is calculated by adding the linear or nonlinear material stiffness $\mathbf{K}_{IJ}^{E}$ to the differential stiffness $\mathbf{K}_{IJ}^{D}$,

$$\mathbf{K}_{IJ}^{(b)} = \mathbf{D}_{bd}^{(b)} \left(\mathbf{K}_{IJ}^{E(d)} + \mathbf{K}_{IJ}^{D(d)} \right) \mathbf{D}_{bd}^{(b)T} \tag{19}$$

The linear or nonlinear material stiffness $\mathbf{K}_{IJ}^{E}$ contains the terms due to the variation of the stresses. The differential stiffness contains the terms due to the variation of the strains, it is often called the geometric stiffness. The linear stiffness or nonlinear material stiffness is

$$\mathbf{K}_{IJ}^{E} = \mathbf{P}_{KI}^{T} \overline{\mathbf{K}}_{KL} \mathbf{P}_{LJ} \tag{20}$$

with

$$\overline{\mathbf{K}}_{KL} = \frac{\partial \overline{\mathbf{f}}_K}{\partial \overline{\mathbf{d}}_L} \tag{21}$$

The differential stiffness is

$$\mathbf{K}_{IJ}^{D} = -\boldsymbol{\Gamma}_I \mathbf{F}_J^T - \mathbf{F}_I \boldsymbol{\Gamma}_J^T + \boldsymbol{\Gamma}_I \boldsymbol{\Psi}_K^T \mathbf{F}_K \boldsymbol{\Gamma}_J^T \tag{22}$$

where $\mathbf{F}_I$ is the matrix of the internal forces

$$\mathbf{F}_I = \begin{bmatrix} spin(\mathbf{n}_I) \\ \frac{1}{2} spin(\mathbf{m}_I) \end{bmatrix} [6,3] \tag{23}$$

and $\boldsymbol{\Gamma}_J$ contains the derivatives of the element rigid body rotation $\boldsymbol{\omega}_D$ with respect to the deformations $\mathbf{d}_J$,

$$\boldsymbol{\Gamma}_J = \begin{bmatrix} \frac{\partial \boldsymbol{\omega}_D}{\partial \mathbf{u}_J} \\ \frac{\partial \boldsymbol{\omega}_D}{\partial \boldsymbol{\omega}_J} \end{bmatrix} [6,3] \tag{24}$$

and $\boldsymbol{\Psi}_K$ is the matrix of rigid body rotations

$$\boldsymbol{\Psi}_K = \begin{bmatrix} -spin\ \mathbf{x}^K \\ \hline \mathbf{I} \end{bmatrix} [6,3] \tag{25}$$

The tangent stiffness is valid for large overall deformations and small element distortions. The formula for the tangent stiffness (18) has been verified with a numerical experiment. Let us assume that the internal forces $\mathbf{f}_I$ are correct. Then we may generate an accurate

tangent stiffness from numerical differentiation of the internal forces. From the central difference formula it follows,

$$\tilde{K}_{ij} = \frac{\partial f_i}{\partial d_j} \approx \frac{1}{2} \frac{f_i(d_j + \Delta d_j) - f_i(d_j - \Delta d_j)}{\Delta d_j} \qquad i,j = 1,...6 * N \tag{26}$$

The numerical experiment was performed in MSC/NASTRAN with a DMAP alter, see MSC/NASTRAN User's Manual [6].

It has been found that the improved tangent stiffness $\mathbf{K}_{IJ}$ (19) in Version 68 matches the numerically generated tangent stiffness with sufficient accuracy. To the contrary, the tangent stiffness in Version 67.5 and earlier does not compare well to the numerically generated tangent.

Examples

Linear Buckling Analysis of a Cylinder.

The lowest buckling load of a cylinder is calculated with MSC/NASTRAN Version 67.5 and Version 68. The numerical solutions are compared with an exact solution from Flügge [7]. The geometry and material data of the cylinder are summarized in Figure 2. The cylinder is discretized with QUAD4 elements. For convenience, we use Sol 77, linear buckling with cyclic symmetry. The buckling load is calculated for different wall thicknesses. The results are summarized in Table 1 and Figure 3.

In Version 67.5, spurious modes occur as the wall of the cylinder becomes thin. With the improved differential stiffness in Version 68, the buckling analysis is free of spurious modes. The eigenvalues of Version 68 indicate a slight stiffening effect compared to Version 67.5.

Linear Buckling Analysis of a Cantilever.

The stiffening effect is illustrated with a cantilever beam, see Figure 4. The cantilever is modeled with QUAD4 elements. The lowest Euler buckling load is calculated for subsequent mesh refinements, the error compared to the exact solution is summarized in Figure 5. In Version 67.5, the differential stiffness produces very accurate results for coarse meshes. Using only one QUAD4 element, the error in the buckling load is 1.5 % in Version 67.5 whereas the improved differential stiffness in Version 68 overestimates the buckling load by more than 20 %.

In engineering analysis, reliable behavior of the elements for fine meshes is considered to be more important than accurate answers for coarse meshes. Therefore, it has been decided to make the new differential stiffness the default in Version 68. The user may still activate the old differential stiffness of Version 67.5 and earlier by overwriting the default with a system cell.

Linear Buckling Analysis in Version 67.5 and Earlier.

In Version 67.5 and earlier, an approximation of the new differential stiffness can be constructed with the following procedure. Every element has to be replaced by two overlapping elements. One element has only membrane properties, MID2 and MID3 are blank on the PSHELL bulk data entry. The other element has only bending properties, MID1 is blank on the PSHELL bulk data entry. This procedure is recommended for linear buckling of thin shells using Version 67.5 and earlier.

Geometric Nonlinear Analysis of a Thin Plate

The bending of a thin plate is analyzed, see Figure 6 for geometry and material data. We use MSC/NASTRAN's nonlinear solution sequence with geometric nonlinear capability, Sol 106 with PARAM,LGDISP,1 in the bulk data. The example has been used to tune the penalty stiffness of the 6th degree of freedom for plates, see [8]. The plate is loaded with a single force. The initial lateral stiffness of the plate is very small. The system becomes stiffer when the lateral displacements increase, see Figure 7. We solve the problem with two different iteration methods. In the first analysis, we use the default iteration method AUTO on the NLPARM bulk data entry. With the improved differential stiffness in Version 68, the number of iterations is reduced by more than half compared to Version 67.5, see Table 2. In the second analysis, we use the full Newton method (ITER,1). In Version 68, the algorithm converges within 3 to 4 iterations per load step after the first load step. In Version 67.5, the algorithm does not converge in the first load step. If the calculation is continued, Version 67.5 diverges at 22.3 % of the final load. The example illustrates how convergence in Version 68 improves for geometric nonlinear analysis as compared to Version 67.5.

In the nonlinear solution sequences of MSC/NASTRAN, Gimbal angle or rotation vector definition may be used for the rotational degrees of freedom. The new approach for geometric nonlinear analysis in Version 68 works for both types of rotations.

Conclusions

MSC/NASTRAN's linear buckling and geometric nonlinear capability for shell elements has been improved in Version 68. The internal forces and the tangent stiffness of the QUAD4 and TRIA3 shell elements are corrected without changing the behavior of the elements for small deformations. The old differential stiffness formulation of Version 67.5 and earlier may be activated in Version 68 by overwriting the default in a system cell.

The shell elements in Version 68 are improved in two areas as compared to Version 67.5 and earlier. In linear buckling, the shell elements are free of spurious modes for thin shells. In geometric nonlinear analysis, the shell elements converge better. Furthermore, the internal forces in Version 68 are in equilibrium in the deformed configuration.

Acknowledgements

The author wants to thank Robert Harder, Chief Scientist of The MacNeal-Schwendler Corporation, for his valuable contributions to this project and his encouragement. Robert Harder wrote the DMAP alter for the tangent stiffness verification, he calculated the exact solution of the buckling load for the cylinder. Furthermore, he found the cure how to avoid spurious modes in linear buckling for Version 67.5 and earlier. The author acknowledges the help of Dae Song of The MacNeal-Schwendler Corporation for coding the element subroutines. Furthermore, the author wants to thank Dave Wallerstein of The MacNeal-Schwendler Corporation for his guidance and encouragement througout this project.

References

1. MacNeal,R.H., " Critique of MSC/NASTRAN Large Displacement Capability ", MSC/NASTRAN Memo RHM-124B, The MacNeal-Schwendler Corporation, Los Angeles, CA, August 30, 1991.

2. Nour-Omid,B. and Rankin,C.C., " Finite Rotation Analysis and Consistent Linearization Using Projectors ", *Computer Methods in Applied Mechanics and Engineering* 93, 353-384, 1991.

3. Rankin,C.C. and Nour-Omid,B., " The Use of Projectors to Improve Finite Element Performance ", *Computers& Structures*, Vol.30, No.1/2, pp.257-267, 1988.

4. Crisfield,M.A., " Nonlinear Finite Element Analysis of Solids and Structures ", Vol.1: Basic Formulations, John Wiley & Sons, 1991.

5. Hoff,C.C., " Software Requirement Specification for the QUAD4 Differential Stiffness ", MSC/NASTRAN Memo CCH-8, The MacNeal-Schwendler Corporation, Los Angeles, CA, January 1993.

6. MSC/NASTRAN User's Manual, Version 67, The MacNeal-Schwendler Corporation, Los Angeles, CA, July 1992.

7. Flügge,W., *Stresses in Shells*, 2nd Ed., Springer-Verlag New York Heidelberg Berlin, 1973.

8. MSC/NASTRAN Handbook for Nonlinear Analysis, based on Version 67, ed. S.H.Lee, The MacNeal-Schwendler Corporation, Los Angeles, CA, March 1992.

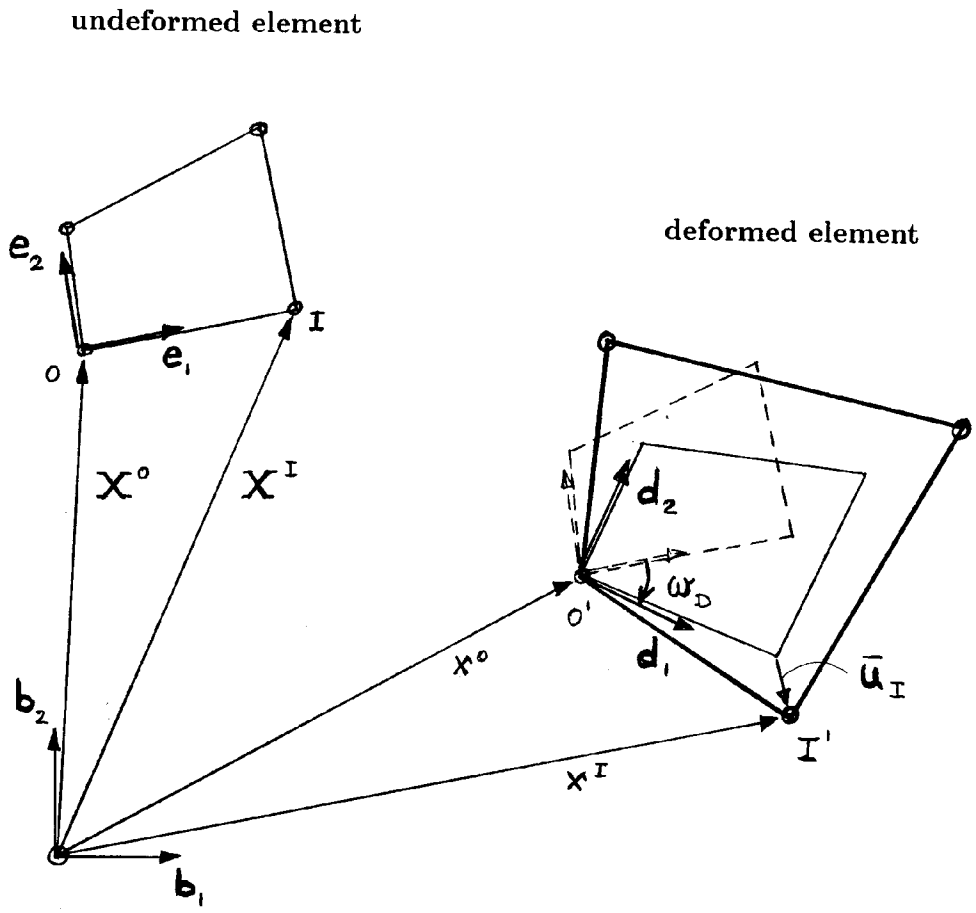

Figure 1. Element net deformations in MSC/NASTRAN

Geometry

Length	L	=	20
Radius	R	=	10
Thicknesses	t	=	1.0, 0.3, 0.1, 0.03

Material

Young's Modulus	E	=	1.0E+7
Poisson's Ratio	ν	=	0.3

Load

Axial load $P\ [\frac{force}{length}]$

FE Model

Cyclic Symmetry	Sol 77, axisymmetric
72 segments,	$\Delta\theta = 5.0\ [degr.]$
20 QUAD4 elements,	$\Delta L = 1.0$

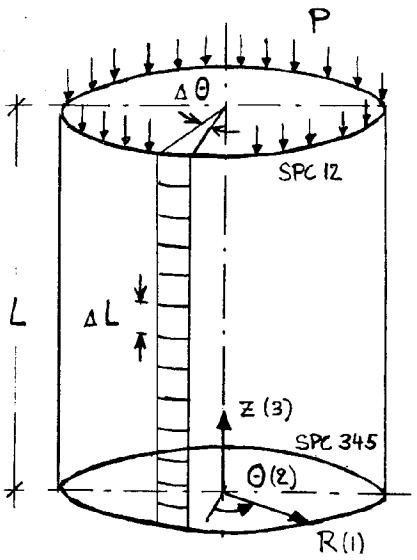

Figure 2. Cylinder under axial load.

thickness t	buckling loads $P_{exact}[\frac{force}{length}]$ see Flügge [7]	P_{num}/P_{exact} Version 67.5	P_{num}/P_{exact} Version 68
1.00	186,186.0 H=2	1.0062	1.0067
0.30	21,206.4 H=3	1.0528	1.0533
0.10	2,740.8 H=4	spur	1.0191
0.03	251.7 H=5	spur	1.0313

H=5 indicates that the lowest buckling load is in harmonic 5.

spur indicates spurious modes.

Table 1. Lowest linear buckling load of a cylinder for various shell thicknesses. 72 segments, 20 QUAD4 elements per segment.

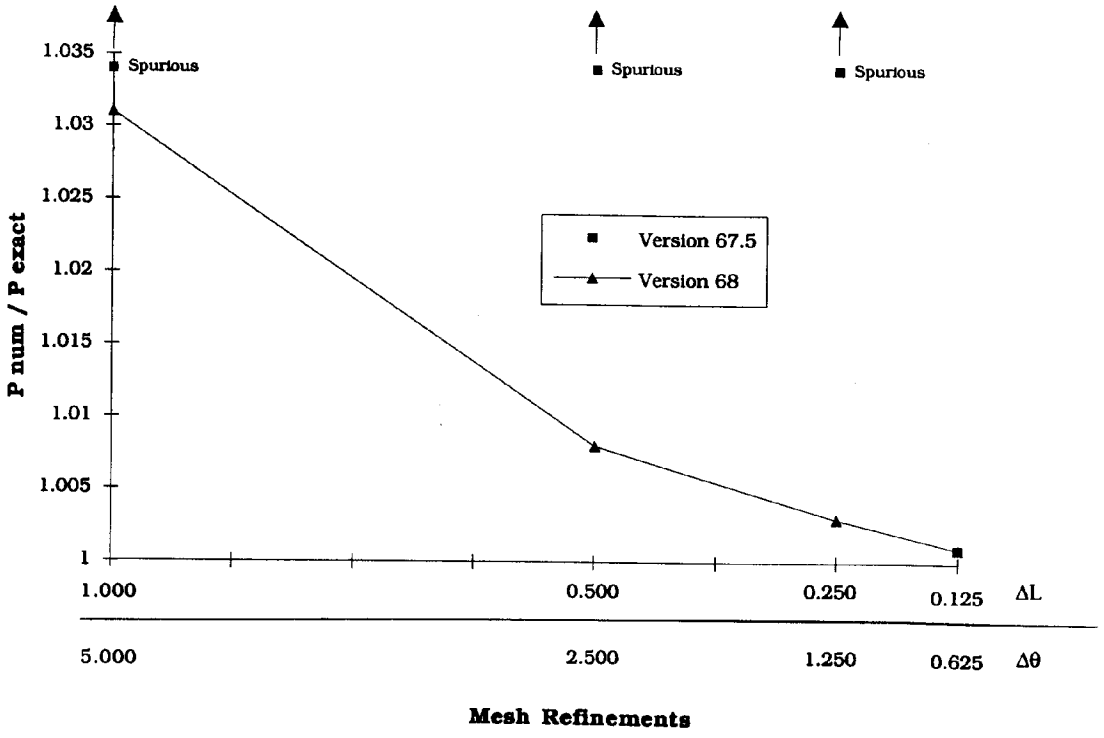

Mesh Refinements

no.of elements	20	40	80	160
no.of segments	72	144	288	576
ΔL	1.000	0.500	0.250	0.125
$\Delta\theta$ [degr.]	5.000	2.500	1.250	0.625

Figure 3. Accuracy in lowest linear buckling load of the cylinder.

Geometry

Length	L	=	12.0
Width	b	=	1.0
Thickness	t	=	0.15

Material

Young's Modulus	E	=	2.0E+7
Poisson's Ratio	ν	=	0.0

Exact solution

Lowest Buckling Load	$\mathbf{P}_{crit}$	=	96.38286

FE Model

1, 2, 4, 8, 16, 32 QUAD4 elements,

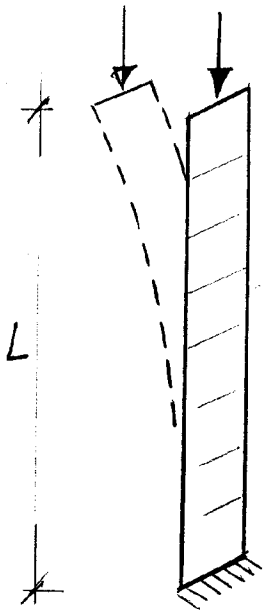

Figure 4. Euler buckling of a cantilever.

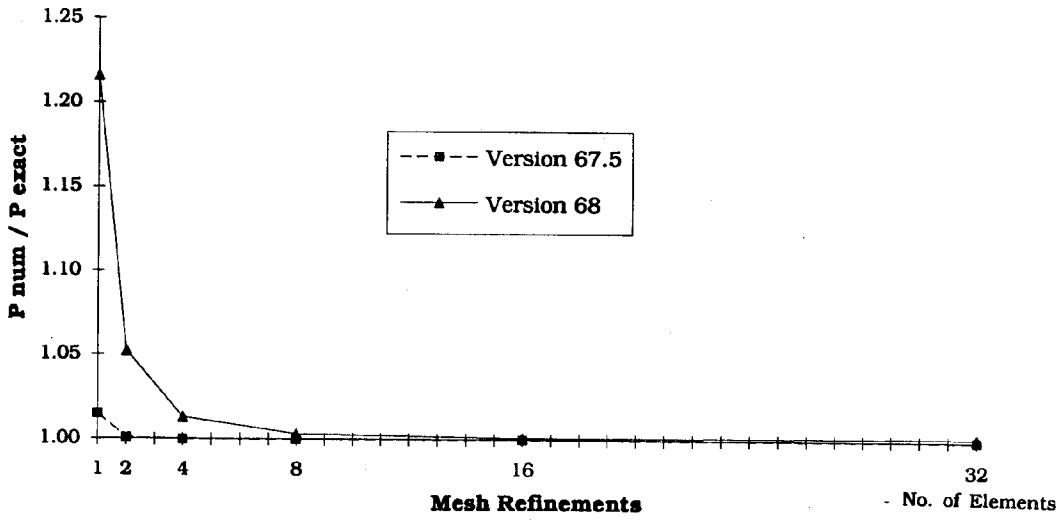

Figure 5. Error in lowest buckling load of the cantilever.

Geometry

Square plate	L	=	400 mm	Young's Modulus	E	=	$2.07E+5$ $[N/mm^2]$
Thicknesses	t	=	0.4 mm	Poisson's Ratio	ν	=	0.3

Load

Concentrated load at grid 19 in negative z-dir.	P	=	13,200.0 [N]

FE Model

4x4 QUAD4 elements	1. Subcase	P	= 2,200.0 [N]
	4 load increments		
	2. Subcase	P	= 13,200.0 [N]
	5 load increments		

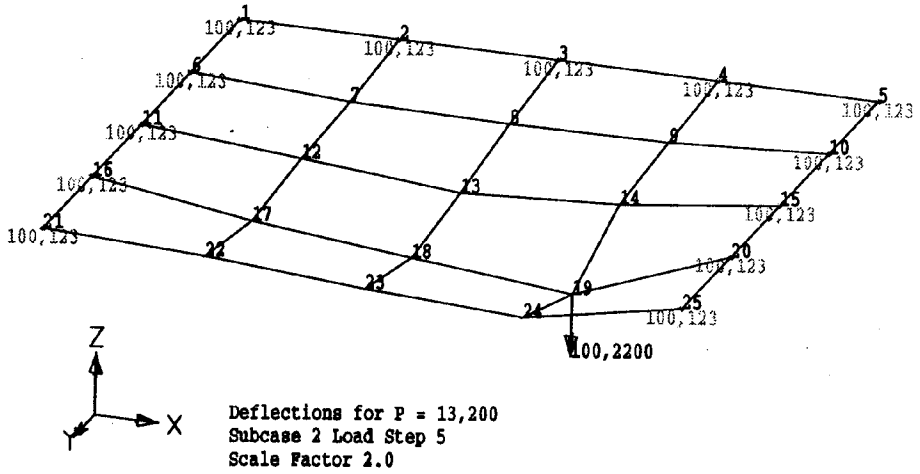

Figure 6. Geometric nonlinear bending of a thin plate.

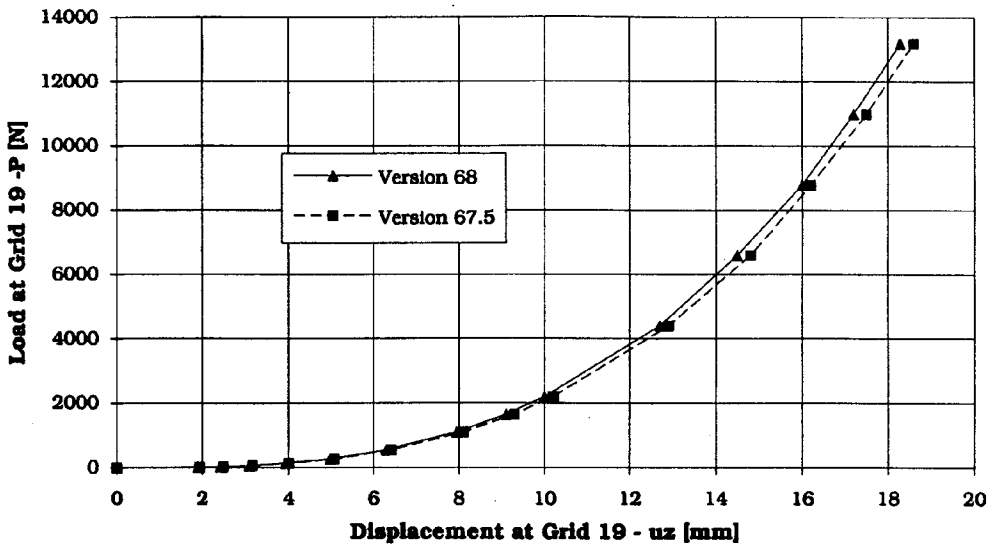

Figure 7. Load versus displacement at grid 19.

Iteration method AUTO (default)

	Version 67.5	Version 68
no.of bisections	5	5
no.of iterations	**185**	**90**
no.of stiffness updates	14	14
displacement at grid 19	-1.859432E+01	-1.826097E+01

Iteration method ITER, 1 (full Newton)

	Version 67.5	Version 68
	diverges at 22.3 % of end load	**converges**
displacement at grid 19	****	-1.826100E+01

Table 2. Number of iterations for bending of a thin plate.